HHS Public Access

Author manuscript

Mol Imaging Biol. Author manuscript; available in PMC 2018 April 05.

Published in final edited form as:

Mol Imaging Biol. 2014 October ; 16(5): 661–669. doi:10.1007/s11307-014-0727-2.

A High-Affinity Near-Infrared Fluorescent Probe to Target Bombesin Receptors

Ajay Shrivastava, **Haiming Ding**, **Shankaran Kothandaraman**, **Shu-Huei Wang**, **Li Gong**, **Michelle Williams**, **Keisha Milum**, **Song Zhang**, and **Michael F. Tweedle**

Department of Radiology, The Ohio State University, Columbus, OH, 43210, USA

Abstract

Purpose—This study aimed to create new optical surgical navigation NIRF probes for prostate and breast cancers.

Procedures—IR800-linker-QWAVGHLM-NH_2 with linker = GSG, GGG, and G-Abz4 were synthesized and characterized. IC_{50} for bombesin receptors (BBN-R) in PC-3 prostate and T47D breast cancer cells, fluorescence microscopy in PC-3 cells, and NIRF imaging in mice PC-3 tumor xenografts were studied.

Results—GGG, GSG, and G-Abz4 derivatives had IC_{50} (nM) for BBN-R+ PC-3 cells=187±31, 56 ±5, and 2.6±0.2 and T47D cells=383±1, 57.4±1.2, and 3.1±1.1, respectively. By microscopy the Abz4 derivative showed the highest uptake, was competed with by BBN, and had little to no binding to BBN-R− cells. In NIRF imaging the G-Abz4 probe was brighter than GGG probe in BBN-R+ tissues in vivo and tissues, tumors, and tumor slices ex vivo. Uptake could be partially blocked in BBN-R+ pancreas but not visibly in tumor.

Conclusions—Linker choice can dominate peptidic BBN-R binding. The G-Abz4 linker yields a higher affinity and specific BBN-R binder in this series of molecules.

Keywords

Optical; Surgical navigation; Near-infrared fluorescent; Gastrin-releasing peptide; AMBA; Bombesin; NIRF; IR800CW

Introduction

Interest in receptor targeted near-infrared fluorescence (NIRF) imaging is growing because of its potential use in image-guided surgery (optical surgical navigation) [1]. Using probes that fluoresce in the NIR (650–850 nm) minimizes tissue auto-fluorescence seen at lower (<600 nm, e.g., hemoglobin) and higher (>900, e.g., water and lipids) wavelengths. NIRF probes are not radioactive, allow real-time imaging, and have a limit of detection ≤1 nM that

Correspondence to: Michael Tweedle; michael.tweedle@osumc.edu.
Ajay Shrivastava and Haiming Ding contributed equally to this work

Electronic supplementary material The online version of this article (doi:10.1007/s11307-014-0727-2) contains supplementary material, which is available to authorized users.

Conflict of Interest. The authors declare that they have no conflict of interest.

allows receptor imaging. These advantages have spurred advances in the development of new fluorescent dyes, molecular targeting probes, and equipment [2–4]. The most popular dyes available for NIRF imaging are organic cyanine molecules with molecular weights ~1,000 Da and excitation/emission at 700–830 nm [3]. One of the most widely used NIRF dyes is IRDye®800CW (IR800). It has high water solubility and stability, demonstrated low toxicity, high relative brightness [3], low albumin binding [5], and is available commercially [3, 4, 6]. There are several IR800 NIRF probes published for imaging targets on human tumor cells: EGFR [7, 8], EGFR-2 [9], VEGF [9, 10], GLUT [11, 12], PSMA [13, 14], CXCR4, and CXCR7 [15], and tumor vasculature, e.g., CD-105 [16], phosphatidylserine [17], phosphatidylethanolamine [18], and integrins [19].

Several hormone peptide receptors are well validated as human cancer cell targets, among them is the bombesin receptor (BBN-R) family [20, 21]. There are four known subtypes of BBN-R that belong to the 7-transmembrane G-protein coupled receptor superfamily (GPCR), including GRPr (gastrin-releasing peptide receptor, BB2 or BRS-2), NMB-R (neuromedin B receptor, BB1 or BRS-1), an orphan receptor BB3-R (BRS-3), and the amphibian receptor BB4-R. Ligands are known for the first two in mammals, but not for the last two [22]. GRPr, and sometimes NMB-R, are well documented in prostate, breast, gastrointestinal stromal, small-cell lung [23–28], and head and neck tumors [29], and over-expression of BBN-R is reported in the tumor vasculature (but not cancer cells) of ovarian and urinary tract cancers [28, 30]. We have previously used DO3A-CH_2CO-G-ABz4-QWAVGHLM-NH2, (AMBA) labeled with ^{177}Lu for radiotherapy [31] and ^{68}Ga has been reported [32] for imaging of GRPr and NMB-R-positive PC-3 tumors. AMBA is comprised of amino acids 7–14 of bombesin (t-BBN), a 4-aminobenzoyl linker (G-Abz4), and 1, 4, 7, 10-tetraazadodecaundecane-1, 4, 7, 10-tetraacetic acid (DO3A) for radio-labeling with metal ions. AMBA binds GRPr and NMB-R avidly (IC_{50}=2–5 nM) with or without a chelated metal ion. AMBA binds *in vivo* to BBN-R+ xenograft tumors and BBN-R-rich normal pancreas in mice. During our work with AMBA, a large variety of compounds with different linkers were synthesized to determine optimal characteristics for systemic radiotherapy, including high tumor uptake and retention, and favorable dosimetry. Target binding and biodistribution were found to be dependent on the structure of the linker used for coupling t-BBN with DO3A. AMBA was found to be one of the best molecules because of its G-Abz4 linker (Fig. 1). Several publications have recently also shown that binding of t-BBN to BBN-R, as well as other ligands of GPCR, is highly dependent on the linker structure [33–35].

Two NIRF agents for targeting BBN-R have been recently reported. The first used a GSG linker (G = glycine, S = serine) between t-BBN and a carbocyanine NIRF dye [36]. The second used a GGG linker between t-BBN and an Alexafluor 680 (AF680) NIRF dye [37]. In this study, we synthesized and validated three new probes: IR800-G-Abz4-t-BBN, IR800-GGG-t-BBN, and IR800-GSG-t-BBN. The three probes were compared *in vitro* and two of them, the highest affinity (G-Abz4) and lowest affinity (GGG) BBN-R binders were characterized *in vivo*.

Materials and Methods

Peptides

Bombesin (BBN, #20665, >95% pure Pyr-QRLGNQWAVGHLM-NH_2) was purchased from AnaSpec (Fremont, CA USA). Human ^{125}I-Tyr^4-BBN (#NEX258050UC) was purchased from PerkinElmer (Waltham, MA USA). IR800-NHS ester and IR800-COOH were purchased from LI-COR (Lincoln, NE, USA). AMBA was a gift from Bracco, SpA (Bracco Diagnostics, Princeton, NJ, USA). QWAVGHLM-NH_2 (t-BBN) and TSPLNIHNGQKL-N (HN1) were synthesized using the Fmoc solid-phase strategy. Rink amide resin (0.5 mmol/g) was loaded onto a reaction vessel placed on an ABI 433A automated peptide synthesizer or an Aapptec Endeavour 90 peptide synthesizer. For each millimoles of the amine on the resin, protected amino acid (4.0 mmol) was activated with 4.0 mmol of the appropriate coupling agent like HATU/HBTU and 8.0 mmol of DIEA for 5 min and the activated acid was transferred to the amine on the solid phase and the vessel was shaken for 1 h. The peptide along with the protection groups were then released from the resin, a process repeated twice with two 10-ml cocktails containing trifluoroacetic acid (TFA), phenol, tris-isopropylsilane, and water in a ratio of 95:2:2:1, and precipitated into methyl-*tert*-butyl ether. The crude peptide was purified by preparative HPLC on a Shimadzu LC-8A with water/acetonitrile (5–70 % gradient), and the resulting product was pooled and freeze dried.

The purified peptide (>95 % pure by HPLC) was then conjugated to IR800-NHS ester. A solution of IRdye800CW-NHS ester (5.0 mg, dissolved in 50 μl DMSO and 50 μl acetonitrile) was added to 4.1 mg of G-Abz4-t-BBN in 500 μl sodium bicarbonate solution (0.1 M) at 0 °C. The resultant mixture was warmed to ambient temperature overnight and monitored by LC/MS (MALDI). The product was isolated by preparative HPLC on a Sunfire (Waters) C18 (30×250 mm, 5 μm) column with 30 ml/min flow rate. The solvent system consisted of the solvent A (0.1 % TFA in water) and B (0.1 % TFA in acetonitrile) with gradient of solvent B ascending from 5 to 65 % over 60 min. The final compound was collected and lyophilized to afford a greenish blue product weighing 1.7 mg. Other IR800 compounds in Table s1 (supplemental Fig. and Table are identified with the prefix, s) were made using the same method.

Analysis of the purity of all of the synthesized peptides was performed using a Shimadzu LC-10ATvp model, Waters C18-RP analytical column (Xterra cartridge, 50×4.6 mm; flow rate=3 ml/min) starting at 95:5 buffer A/buffer B and then linear gradient over 10 min to 30:70 buffer A/buffer B. For HN1, a control peptide [38], the gradient system was the same but ran only from 5–50 % buffer B. The purity was >95 % by relative HPLC peak area at 220 nm. HPLC traces are shown in Fig. s1.

The dye conjugates were characterized for identity by matrix-assisted laser desorption/ionization time-of-flight (MALDI-TOF; Table s1).

Cell Culture

Human prostate cancer cells, adenocarcinoma (PC-3) from American Type Culture Collection (ATCC) cat # CRL-1435, human mammary gland ductal cancer cells (T47D) cat # CRL-2865, and human breast cancer cells (HCC 1937) cat # CRL-2336 were maintained

in DMEM (Invitrogen, Carlsbad, CA), high glucose supplemented with 10 % fetal bovine serum (Atlanta Biologicals, Flowery Branch, GA USA), an additional 2 mM L-glutamine solution (Sigma-Aldrich, St. Louis, MO, USA), and 1 % Pen Strep (Invitrogen), at 37 °C with 5 % CO_2. The cell lines were sub-cultured using 0.25 % trypsin (Invitrogen) twice per week. Cells were seeded in 96-well plates at ~30,000 cells per well (counted on a Invitrogen Countess) in 200 μl of cell culture medium for competition assays, and eight-well collagen coated chamber slides at ~70,000 cells per chamber in 300 μl of cell culture medium for direct assays.

Competition Radioligand Binding

Cell culture medium was removed 24 h after plating and cells were washed twice with binding buffer (RPMI 1640, 20 mM HEPES, 0.1 % BSA *w/v*, 0.5 mM PMSF, 0.1 mg/ml bacitracin) at room temperature (RT). Cells were placed in a 4 °C refrigerator for 30 min for slow cooling. All the subsequent steps used ice cold solutions and incubations were performed at 4 °C. Peptide mixtures for the competition assay were prepared using a constant concentration of ^{125}I-Tyr^4-BBN (0.22 μCi/ml), and a varied (0.1 nM – 1 μM) concentration of competing peptide. Cells were incubated with 70 μl of peptide mixtures in each well for 1 h. Each concentration of competing peptide was tested in triplicate. After 1 h, cells were washed five times with ice-cold wash buffer (25 mM HEPES, 150 mM NaCl, pH 7.4). Cells were lysed by adding 200 μl of 1 N NaOH kept at 37 °C, twice to each well. Solutions were transferred to tubes and radioactivity was measured using an automatic gamma counter (PerkinElmer Wizard II, Model 2480). Data were analyzed using GraphPad Prism 5. The data are reported as mean ± the *SE*.

Direct Binding Assays in Cells

Cell culture medium was removed from eight-well chamber slides 24 h after plating and cells were washed twice with binding buffer at RT, then left in binding buffer at RT for 30 min. Peptide and control dye solutions were prepared by diluting 250 μM stock solution of peptides and control dye in 50 % DMSO to 2 μM final concentration in the binding buffer. Cells were incubated with 200 μl of peptide solutions or control dye in each chamber. Each peptide was tested in duplicate. After 2 h incubation, cells were washed four times with 300 μl of binding buffer and once with 300 μl of wash buffer (25 mM HEPES/150 mM NaCl at pH 7.4) containing 1 μg/ml 4′, 6-diamidino-2-phenylindole (DAPI). After that, the chamber slide scaffold was removed, a drop of aqua-poly/mount was added to each chamber, and chamber slides were cover-slipped and sealed with clear nail polish. Cells were observed and imaged with an Olympus IX81 microscope using an IR800 filter set.

Competition for Direct Binding in Cells

Cells were incubated with 200 μl of peptide mixtures containing 1.5 μM of IR800-G-Abz4-t-BBN and 516 μM of competing peptide, either BBN or control peptide, HN1 (TSPLNIHNGQKL-NH2) [38]. The rest of the assay was the same as the direct cell binding assay.

Animal Experimental Protocols

All animal studies were conducted in compliance with animal protocols approved by The Ohio State University IACUC, and were conducted within Laboratory Animal Resource monitored facilities by trained, approved personnel. Animals were housed communally, three to five same-sex animals per cage, given water ad libitum, quarantined 1 week, then fed a diet of chlorophyll-free chow (Harlan Lab, IN, cat # TD.97184) for at least 10 days prior to experiments.

Nude male mice, 4 to 6 weeks old, CrTac:NCr-$_{Foxn1}^{nu}$ homozygous (Taconic Farms Inc.) without xenografts were injected while conscious via tail vein with 5-nmol of test compound in 100 μl of injection buffer (5 % ascorbic acid containing 0.025 % *w*/*v* EDTA, 0.2 mg/ml selenomethionine, and 0.2 % human serum albumin in phosphate-buffered saline (PBS) adjusted to pH 5.8 with NaOH [39]). Animals were imaged at 1–5 and 24 h to grossly observe clearance of the IR800 conjugates. After euthanasia, organs were excised and imaged (Fig. s2–s6).

For pharmacokinetics studies, normal female balb/c mice were injected with 10 nmol IR800-G-Abz4-t-BBN or IR800-GGG-t-BBN (*N*=4 each) in 100 μl injection buffer via tail vein. At 0.5, 1, 3, 6, and 24-h post-injection, 5~10 μl of blood was collected from the saphenous vein and loaded into a black wall 96-well plate containing 100 μl PBS per well. The fluorescence intensity was counted using a synergy H4 hybrid multi-mode microplate reader (BioTech, VT) at 764 nm excitation/809 nm emission, then converted to counts per microliter and further analyzed using GraphPad Prism 5 (GraphPad Software, CA) to calculate the blood clearance halftime (*T*1/2) using a single-phase analysis, which fit better than other models.

PC-3 tumor mice were created from 4- to 6-week old nude male CrTac:NCr-$_{Foxn1}^{nu}$ homozygous mice (Taconic Farms Inc.). The mice were subcutaneously injected with 1×10^7 PC 3 cells in 100 μl of PBS in the left flanks. Tumors were allowed to grow to ~150 mm^3. Each animal was injected with 10 nmol of test compound in 100 μl of injection buffer.

Imaging experiments performed in the PC-3-tumor-bearing mice used 10 nmol of IR800-G-Abz4-BBN or IR800-GGG-t-BBN injected with (*N*=3) or without (*N*=3) an additional 100 nmol of ABMA [31]. Animals were euthanized at 3-h post-administration and tumors and pancreata were excised and imaged. Pancreata were similar in size among the animals and were imaged in a flattened state and piled into a ball approximating the diameter of a tumor. Tumors were imaged as extracted, then in two cases where paired animals had different sized tumors, the larger tumors were trimmed with a scalpel to equalize the tumor masses.

Near Infrared Fluorescence Imaging

Whole animal and *ex vivo* organ images were collected using both a CRi Maestro white light excitation imager (CRi Inc., Woburn, MA, USA) and a laser excitation Fluobeam™ 800 NIR imaging system (Fluoptics, Grenoble, France). The Fluobeam system excites with a 780-nm emission laser and records with a CCD camera with >800 nm emission filtering. Imaging by a CRi system was performed using the NIR filter and multi-filter acquisition mode from 740–950 nm with 10 nm increments. The 23 spectra were separated using the instrument's software. We used an uninjected mouse and the board supporting the animal

and organs as background. The mice were euthanized immediately prior to imaging. Whole body images were taken after skinning the mice. Organs were then dissected and laid out for *ex vivo* imaging. The images were also captured with the tumors sliced 2-mm thick with surgical scarf. Comparisons of animals and tissues were made by placing the compared animal or tissue set in the same image to equalize exposure times.

Statistical Analysis

To compare the fluorescence intensity in the blood between animals injected with IR800-G-Abz4-t-BBN and IR800-GGG-t-BBN at various time points, a *t* test was utilized. *P* values <0.05 were considered as significant.

Results

The structures of the three new molecules are shown in Fig. 1. The amino acid sequences and analytical data are in Table s1. HPLC confirmed compound purity to >95 % and MALDI mass spectra confirmed the identity. PC-3 and T47D cells are known to over-express human GRPr (BB2) [31] and were used for the competition assays using ^{125}I-Tyr^4-BBN, a well-established GRPr binding radioligand [40]. The competition binding curves of the three conjugates and BBN, the positive control, are shown in Fig. 2, and the IC_{50} values are listed in Table 1. The BBN control IC_{50} values in both cell lines were in agreement with literature. Overall, the IC_{50} data span a range 400 nM with only the G-Abz4-linker producing a peptide conjugate that approached the BBN IC_{50}=1–2 nM. While all three conjugates could be categorized as positive binders, the G-Abz4-linked conjugate had IC_{50} values 20–100-fold greater than the GGG- and GSG-linked conjugates.

A similar binding affinity pattern was observed in the direct cell binding assays (Fig. 3). IR800-GGG-t-BBN, IR800-GSG-t-BBN, and IR800-G-Abz4-t-BBN bound to PC-3 cells to widely different extents (Fig. 3a). The peptides appeared to be internalized, based on the proximity of the observed 800 nm dye signal to the DAPI-stained nuclei. Internalization would be expected of the agonist t-BBN targeting peptide [31]. There was no binding or internalization observed with the IR800-carboxylate dye control. The IR800-G-Abz4-t-BBN showed the highest overall signal among the compounds as expected from the IC_{50} data. In Fig. 3b, it can be seen that the binding of IR800-G-Abz4-t-BBN to PC-3 cells was specifically blocked by excess BBN (~345-fold) peptide but not by the same amount of the unrelated HN1 peptide (Fig. 3b, top), demonstrating the specific nature of the binding. In addition, the IR800-G-Abz4-t-BBN did not bind to HCC1937 cells, a breast cancer cell line that does not express significant BBN-R (Fig. 3b, bottom, Wang *et al.* [41]).

Initially, the binding of IR800-G-Abz4-t-BBN was tested in a nude mouse without a xenograft tumor, as BBN-R are present in pancreas [31]. Renal excretion was indicated by high signal in the bladder (e.g., Figs. s3–4) at early times (3–4 h) that persisted at 24 h in whole body images. This route has previously been shown to be predominant for AMBA [31], a DO3A-counterpart of IR800-G-Abz4-t-BBN, as well as for the carboxylate of IR800 [42]. Despite rapidly accumulating and bright signal in the bladder, most tissues remained very bright in the early time images for all agents as the agents cleared, similar to other peptides labeled with IR800 [42, 43]. No signs of gross toxicity were observed at 5–40 nmol

intravenous doses. Excised BBN-R+ pancreas and BBN-R− muscle tissues from the G-Abz4- and GGG-linked peptides at 3-h post-intravenous dose demonstrated (Fig. s5) relatively low muscle signal for both compounds, but a clear preference for the BBN-R-rich pancreas over muscle for the G-Abz4-linked peptide, and a barely visible difference in pancreas and muscle for the GGG-linked peptide.

Blood concentration vs time curves for the GGG- and the G-Abz4-linked compounds were similar with a half-life for blood clearance of 1.7 and 2.6 h, respectively (Fig. 4a). From 1 to 24 h, only the 3 and 6 h time points were significantly different ($P<0.05$), with the GGG derivative lower in blood concentration. We chose 24 h imaging to compare the two molecules based upon earlier work with AMBA [40] in the same mouse model. Our PC-3 cell studies and blood curves indicated similar behavior of IR800-Abz4-t-BBN and AMBA, and the two fluorescent molecules we compared *in vivo* coalesced in blood concentration at 24-h post-administration. Another study ^{111}In(chelate)-labeled t-BBN also found 24 h to have the highest tumor uptake [44]. Whole body 24 h images in PC-3 xenograft mice are shown in Fig. 4b. Salient features are visible in both CRi and Fluobeam images, but the CRi processed images appear to emphasize the feet (skin) and tail vein (injection site). IR800-G-Abz4-t-BBN-treated mice showed tumor well above background, while IR800-GGG-t-BBN-treated mice showed only spleen and kidneys. Euthanasia at 24 h, and extraction of BBN-R-positive pancreas, PC-3 tumor, and muscle (BBN-R−), gave the images in Fig. 4c. The GGG-linked peptide barely demonstrated the relative brightness of the BBN-R-positive tissues over muscle. In contrast, for the G-Abz4-linked conjugate, the images clearly demonstrate high contrast and brightness in pancreas and PC-3 tumor tissue compared to muscle. To place the images on a semi-quantitative footing with similar attenuation in tissue we sliced the tumors into 2-mm slabs and imaged again (Fig. 4d) with the same results. We also saw intra-tumor heterogeneity of signal in mice dosed with IR800-G-Abz4-t-BBN. This was best visualized with the Fluobeam images.

To demonstrate specific binding, 10 nmol doses of IR800-peptide were coinjected with 100 nmol of AMBA, a non-fluorescent analog. AMBA is a well-studied BBN-R agonist (BB1 and BB2) with IC_{50}=2–5 nM (vs 2 nM for BBN) in the same assay as in Fig. 2. Solubility limited the AMBA dose, but the data in Fig. 5 still indicate that 100 nmol was enough to demonstrate reduction in the signal of the pancreas by co-injected AMBA. Tumors were resistant to receptor blockade by 100 nmol AMBA.

We observed heterogeneous tumor signal (Figs. 4–6) suggestive of necrosis. In Fig. 6, we show an AMBA blocking experiment, along with the histology slides of the tumor whose signal is shown in the optical images. The H&E histology slides demonstrate the necrotic tissue in the central region of the tumor, accounting for the signal intensity features visible in the sliced tumor tissues.

Discussion

Small molecules are often sought as imaging radiopharmaceuticals because their faster targeting and clearance allows same-day clinical imaging and lower radiation exposure compared to proteins. They are also less expensive to develop for commercial clinical use.

However, the labeling chemistry with >0.5 kDa fluors is more likely to affect the targeting of small (2–5 kDa) molecules than is radiolabeling with a single atom or small moiety. Our data, along with the two published examples of fluor-linked-t-BBN probes (Fig. s7), demonstrates that both linker and fluorescent label structure can dramatically affect t-BBN target binding. It is especially interesting that interchanging two structurally similar bis-cyanine dyes, AF680 and IR800, creates the poorly binding IR800-GGG-t-BBN and the strongly binding AF680-GGG-t-BBN in the same two cell lines (Table 1). A similar difference occurs when IR800CW is substituted for carbocyanine with the GSG linker. IR800 has several additional SO_3H groups and a bulky aromatic ring in the center of its structure, compared to the other dyes, adding charge, probably rigidity and lipophilicity to the overall probe structures, each of which could influence interaction of the adjacent peptide with its receptor. Whatever the specific molecular interaction that reduces the binding strength of IR800-labeled t-BBN when the GGG and GSG linkers are used, the G-Abz4 linker apparently insulates the t-BBN-R binding peptide from it.

Unlike nuclear images of targeted probes, the proposed clinical use of NIRF probes is intraoperative observation of surgical margins and guidance of sampling of excised specimens, and not whole body external imaging. Interpretation of NIRF optical images should, we think, be made qualitatively in our context due to the significant attenuation of light by overlying tissue. We therefore opted not to cite numerical values for the detected light, knowing from experience that altering the animal's position can significantly alter the numbers. Some alleviation of the attenuation affect can be achieved by slicing *ex vivo* imaged tissue as we have done in Fig. 4c and Fig s6, into 2-mm slabs. This also allowed us to observe probe uptake heterogeneity, a feature not unexpected in rapidly growing xenografts, which we confirmed via H&E histology (Fig. 6). Comparing the CRi and Fluobeam images shows some negative effect of the processing by the CRi in the form of granularity.

Initial animal data (Fig. s2–4) demonstrated rapid clearance of the probes mainly through the renal route. Some 24 h retention in the skin was noted, but otherwise the BBN-R-rich pancreas was the normal target organ for the G-Abz4-linked peptide. Unlike solid tissue images, blood data can be quantitatively analyzed using a fluorescence plate reader if it is diluted identically for each sample. The data in Fig. 4a produced significantly ($P<0.05$) though not dramatically different blood clearance half-lives for the GGG and Abz4 derivatives, with both similar in initial clearance to that reported for AF680-GGG-t-BBN (~1 h initial rate). After the initial decline in signal, IR800-GGG-t-BBN appears to clear faster and more completely than the AF680-GGG-t-BBN (1.7 vs 4 h, respectively) [45].

Our data demonstrating the difference in target signal and signal to background between the strongly and weakly bound probes suggests that fairly strong binding is required for this probe molecule to successfully detect its receptors in imaging. Overall, both the lower affinity and the faster blood clearance probably contributed to the poorer tumor imaging of the GGG derivative.

We confirmed that the G-Abz4-linked probe could be visibly competed from its receptor *in vivo*. This was recently reported for the AF680-GGG-t-BBN probe [45]. In studies of

AMBA in PC-3 tumor mice, pancreas and tumor uptake of 0.2 nmol of ^{177}LuAMBA was significantly competed with by co-injection ~50 nmol of unlabeled AMBA [31]. We used unlabeled AMBA to attempt a similar experiment in this work but the conditions in NIRF imaging are not as conducive to receptor blocking experiments as in radiolabel studies because of the 50-fold higher mass dose in NIRF, and the solubility limits of the AMBA and other BBN-R binders that restrict the mass dose of AMBA to 100 nmol. We observed diminished pancreatic signal with AMBA blocking but not obviously diminished tumor signal. The data published on radiolabeled AMBA [31] with the benefit of accurate radiolabeled biodistributions showed that that mice PC-3 tumors contain a 3–4-fold lower concentration of injected ^{177}LuAMBA than the pancreas *in vivo*, but that the tumors resisted unlabeled AMBA saturation *in vivo* while pancreas did not. We therefore feel confident that the binding to these BBN-R+ tissues by IR800-G-Abz4-t-BBN is at least significantly, if not totally receptor specific. Overall, the results suggest that the pancreatic receptors are regulated differently than those expressed on the PC-3 cells.

Conclusion

The t-BBN peptide that binds BBN-R is highly sensitive to changes in the linker that connects it to the fluorescent label, and apparently also to the fluorescent label structure. IR800-G-Abz4-t-BBN is a receptor-specific NIRF probe with strong affinity for its target receptors *in vitro*, and effective *in vitro* and *in vivo* imaging of BBN-R+.

Supplementary Material

Refer to Web version on PubMed Central for supplementary material.

Acknowledgments

Funding sources for this research are The Ohio State University College of Medicine, The Stefanie Spielman Foundation, and NIH 1 S10 RR025660-01A1.

Abbreviations

GRP	Gastrin-releasing peptide
NIRF	Near-infrared fluorescent
BBN	Bombesin
BBN-R	Bombesin receptors
Abz-4	4-aminobenzoic acid

References

1. Nguyen QT, Tsien RY. Fluorescence-guided surgery with live molecular navigation—a new cutting edge. Nat Rev Cancer. 2013; 13:653–662. [PubMed: 23924645]
2. Keereweer S, Sterenborg HJ, Kerrebijn JD, et al. Image-guided surgery in head and neck cancer: current practice and future directions of optical imaging. Head Neck. 2012; 34:120–126. [PubMed: 21284051]

3. Azhdarinia A, Ghosh P, Ghosh S, et al. Dual-labeling strategies for nuclear and fluorescence molecular imaging: a review and analysis. Mol Imaging Biol. 2012; 14:261–276. [PubMed: 22160875]
4. Kovar JL, Simpson MA, Schutz-Geschwender A, Olive DM. A systematic approach to the development of fluorescent contrast agents for optical imaging of mouse cancer models. Anal Biochem. 2007; 367:1–12. [PubMed: 17521598]
5. Berezin MY, Guo KV, Akers W, et al. Rational approach to select small peptide molecular probes labeled with fluorescent cyanine dyes for in vivo optical imaging. Biochemistry-US. 2011; 50:2691–2700.
6. Marshall MV, Draney D, Sevick-Muraca EM, Olive DM. Single-dose intravenous toxicity study of IRDye 800CW in Sprague–Dawley rats. Mol Imaging Biol. 2010; 12:583–594. [PubMed: 20376568]
7. Gong H, Kovar J, Little G, et al. In vivo imaging of xenograft tumors using an epidermal growth factor receptor-specific affibody molecule labeled with a near-infrared fluorophore. Neoplasia. 2010; 12:139–149. [PubMed: 20126472]
8. Qi S, Miao Z, Liu H, et al. Evaluation of four affibody-based near-infrared fluorescent probes for optical imaging of epidermal growth factor receptor positive tumors. Bioconjug Chem. 2012; doi: 10.1021/bc200596a
9. Terwisscha van Scheltinga AG, van Dam GM, Nagengast WB, et al. Intraoperative near-infrared fluorescence tumor imaging with vascular endothelial growth factor and human epidermal growth factor receptor 2 targeting antibodies. J Nucl Med. 2011; 52:1778–1785. [PubMed: 21990576]
10. Wu F, Tamhane M, Morris ME. Pharmacokinetics, lymph node uptake, and mechanistic PK model of near-infrared dye-labeled bevacizumab after IV and SC administration in mice. AAPS J. 2012; 14:252–261. [PubMed: 22391791]
11. Kovar JL, Volcheck W, Sevick-Muraca E, et al. Characterization and performance of a near-infrared 2-deoxyglucose optical imaging agent for mouse cancer models. Anal Biochem. 2009; 384:254–262. [PubMed: 18938129]
12. Levi J, Cheng Z, Gheysens O, et al. Fluorescent fructose derivatives for imaging breast cancer cells. Bioconjug Chem. 2007; 18:628–634. [PubMed: 17444608]
13. Chen Y, Dhara S, Banerjee SR, et al. A low molecular weight PSMA-based fluorescent imaging agent for cancer. Biochem Biophys Res Commun. 2009; 390:624–629. [PubMed: 19818734]
14. Liu T, Nedrow-Byers JR, Hopkins MR, Berkman CE. Spacer length effects on in vitro imaging and surface accessibility of fluorescent inhibitors of prostate specific membrane antigen. Bioorg Med Chem Lett. 2011; 21:7013–7016. [PubMed: 22018464]
15. Meincke M, Tiwari S, Hattermann K, et al. Near-infrared molecular imaging of tumors via chemokine receptors CXCR4 and CXCR7. Clin Exp Metastasis. 2011; 28:713–720. [PubMed: 21735100]
16. Yang Y, Zhang Y, Hong H, et al. In vivo near-infrared fluorescence imaging of CD105 expression during tumor angiogenesis. Eur J Nucl Med Mol Imaging. 2011; 38:2066–2076. [PubMed: 21814852]
17. Zhao D, Stafford JH, Zhou H, Thorpe PE. Near-infrared optical imaging of exposed phosphatidylserine in a mouse glioma model. Transl Oncol. 2011; 4:355–364. [PubMed: 22191000]
18. Stafford JH, Thorpe PE. Increased exposure of phosphatidylethanolamine on the surface of tumor vascular endothelium. Neoplasia. 2011; 13:299–308. [PubMed: 21472134]
19. Ye Y, Zhu L, Ma Y, et al. Synthesis and evaluation of new iRGD peptide analogs for tumor optical imaging. Bioorg Med Chem Lett. 2011; 21:1146–1150. [PubMed: 21251820]
20. Lee S, Xie J, Chen XY. Peptides and peptide hormones for molecular imaging and disease diagnosis. Chem Rev. 2010; 110:3087–3111. [PubMed: 20225899]
21. Reubi JC, Maecke HR. Peptide-based probes for cancer imaging. J Nucl Med. 2008; 49:1735–1738. [PubMed: 18927341]
22. Ohki-Hamazaki H, Iwabuchi M, Maekawa F. Development and function of bombesin-like peptides and their receptors. Int J Dev Biol. 2005; 49:293–300. [PubMed: 15906244]

23. Markwalder R, Reubi JC. Gastrin-releasing peptide receptors in the human prostate: relation to neoplastic transformation. Cancer Res. 1999; 59:1152–1159. [PubMed: 10070977]
24. Reubi JC. Peptide receptors as molecular targets for cancer diagnosis and therapy. Endocr Rev. 2003; 24:389–427. [PubMed: 12920149]
25. Reubi JC, Korner M, Waser B, et al. High expression of peptide receptors as a novel target in gastrointestinal stromal tumours. Eur J Nucl Med Mol Imaging. 2004; 31:803–810. [PubMed: 14985869]
26. Reubi JC, Macke HR, Krenning EP. Candidates for peptide receptor radiotherapy today and in the future. J Nucl Med. 2005; 46:67S–75S. [PubMed: 15653654]
27. Reubi JC, Wenger S, Schmuckli-Maurer J, et al. Bombesin receptor subtypes in human cancers: detection with the universal radioligand ^{125}I-[D-TYR^{6}, β-ALA^{11}, PHE^{13}, NLE^{14}] Bombesin (6–14). Clin Cancer Res. 2002; 8:1139–1146. [PubMed: 11948125]
28. Fleischmann A, Waser B, Reubi JC. Overexpression of gastrin-releasing peptide receptors in tumor-associated blood vessels of human ovarian neoplasms. Cell Oncol. 2007; 29:421–433. [PubMed: 17726264]
29. Lango MN, Dyer KF, Lui VW, et al. Gastrin-releasing peptide receptor-mediated autocrine growth in squamous cell carcinoma of the head and neck. J Natl Cancer Inst. 2002; 94:375–383. [PubMed: 11880476]
30. Fleischmann A, Waser B, Reubi JC. High expression of gastrin-releasing peptide receptors in the vascular bed of urinary tract cancers: promising candidates for vascular targeting applications. Endocr Relat Cancer. 2009; 16:623–633. [PubMed: 19478282]
31. Lantry LE, Cappelletti E, Maddalena ME, et al. 177Lu-AMBA: synthesis and characterization of a selective 177Lu-labeled GRP-R agonist for systemic radiotherapy of prostate cancer. J Nucl Med. 2006; 47:1144–1152. [PubMed: 16818949]
32. Cagnolini A, Chen J, Ramos K, et al. Automated synthesis, characterization and biological evaluation of [(68)Ga]Ga-AMBA, and the synthesis and characterization of (nat)Ga-AMBA and [(67)Ga]Ga-AMBA. Appl Radiat Isot. 2010; 68:2285–2292. [PubMed: 20638858]
33. Fani M, Maecke HR, Okarvi SM. Radiolabeled peptides: valuable tools for the detection and treatment of cancer. Theranostics. 2012; 2:481–501. [PubMed: 22737187]
34. Fani M, Maecke HR. Radiopharmaceutical development of radiolabelled peptides. Eur J Nucl Med Mol Imaging. 2012; 39(Suppl 1):S11–S30. [PubMed: 22388624]
35. Bohme I, Beck-Sickinger AG. Illuminating the life of GPCRs. Cell Commun Signal. 2009; 7:16. [PubMed: 19602276]
36. Achilefu S, Jimenez HN, Dorshow RB, et al. Synthesis, in vitro receptor binding, and in vivo evaluation of fluorescein and carbocyanine peptide-based optical contrast agents. J Med Chem. 2002; 45:2003–2015. [PubMed: 11985468]
37. Ma L, Yu P, Veerendra B, et al. In vitro and in vivo evaluation of Alexa Fluor 680-bombesin[7-14]NH2 peptide conjugate, a high-affinity fluorescent probe with high selectivity for the gastrin-releasing peptide receptor. Mol Imaging. 2007; 6:171–180. [PubMed: 17532883]
38. Hong FD, Clayman GL. Isolation of a peptide for targeted drug delivery into human head and neck solid tumors. Cancer Res. 2000; 60:6551–6556. [PubMed: 11118031]
39. Chen J, Linder KE, Cagnolini A, et al. Synthesis, stabilization and formulation of [177Lu]Lu-AMBA, a systemic radiotherapeutic agent for gastrin releasing peptide receptor positive tumors. Appl Radiat Isot. 2008; 66:497–505. [PubMed: 18178448]
40. Lantry LE, Cappelletti E, Maddalena ME, et al. Lu-177-AMBA: synthesis and characterization of a selective Lu-177-labeled GRP-R agonist for systemic radiotherapy of prostate cancer. J Nucl Med. 2006; 47:1144–1152. [PubMed: 16818949]
41. Wang S-H, Ding H, Shrivastava A, Tweedle MF. Study of Bombesin receptor family in breast cancer cells [abstract]. 2013
42. Choi HS, Nasr K, Alyabyev S, et al. Synthesis and in vivo fate of zwitterionic near-infrared fluorophores. Angew Chem Int Ed Engl. 2011; 50:6258–6263. [PubMed: 21656624]
43. Choi HS, Gibbs SL, Lee JH, et al. Targeted zwitterionic near-infrared fluorophores for improved optical imaging. Nat Biotechnol. 2013; 31:148–153. [PubMed: 23292608]

44. Garrison JC, Rold TL, Sieckman GL, et al. Evaluation of the pharmacokinetic effects of various linking group using the 111In-DOTA-X-BBN(7-14)NH2 structural paradigm in a prostate cancer model. Bioconjug Chem. 2008; 19:1803–1812. [PubMed: 18712899]

45. Cai QY, Yu P, Besch-Williford C, et al. Near-infrared fluorescence imaging of gastrin releasing peptide receptor targeting in prostate cancer lymph node metastases. Prostate. 2013; 73:842–854. [PubMed: 23280511]

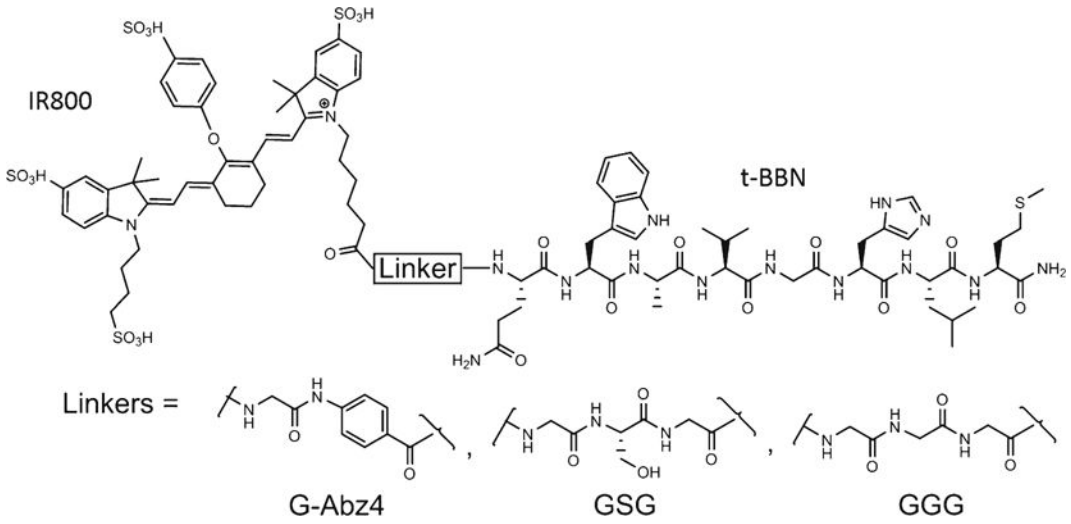

Fig. 1.
Chemical structure of IR800-Linker-t-BBN molecules.

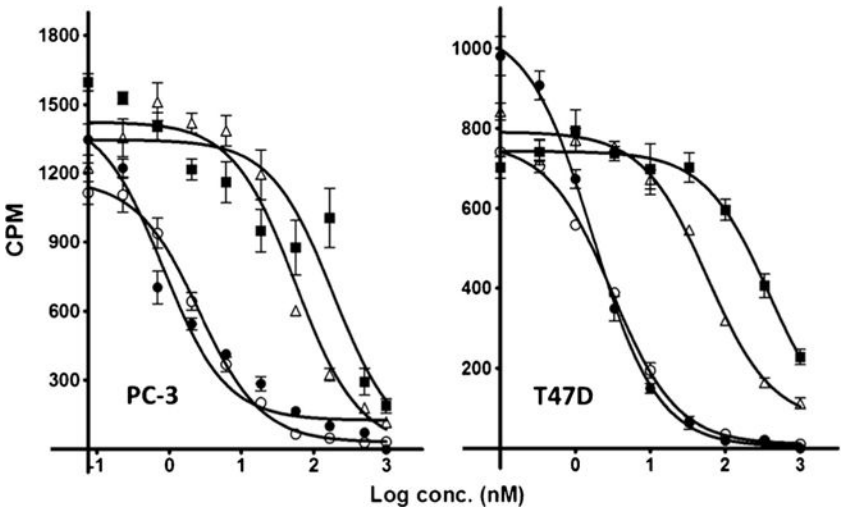

Fig. 2.

Competition between ^{125}I-Tyr4-BBN and BBN-R targeted ligands for binding to PC-3 cells (*left*) and to T47D cells (*right*). BBN (*closed circle*), IR800-G-Abz4-t-BBN (*open circle*), IR800-GSG-t-BBN (*triangle*), and IR800-GGG-t-BBN (*square*). IC_{50} values are in Table 1.

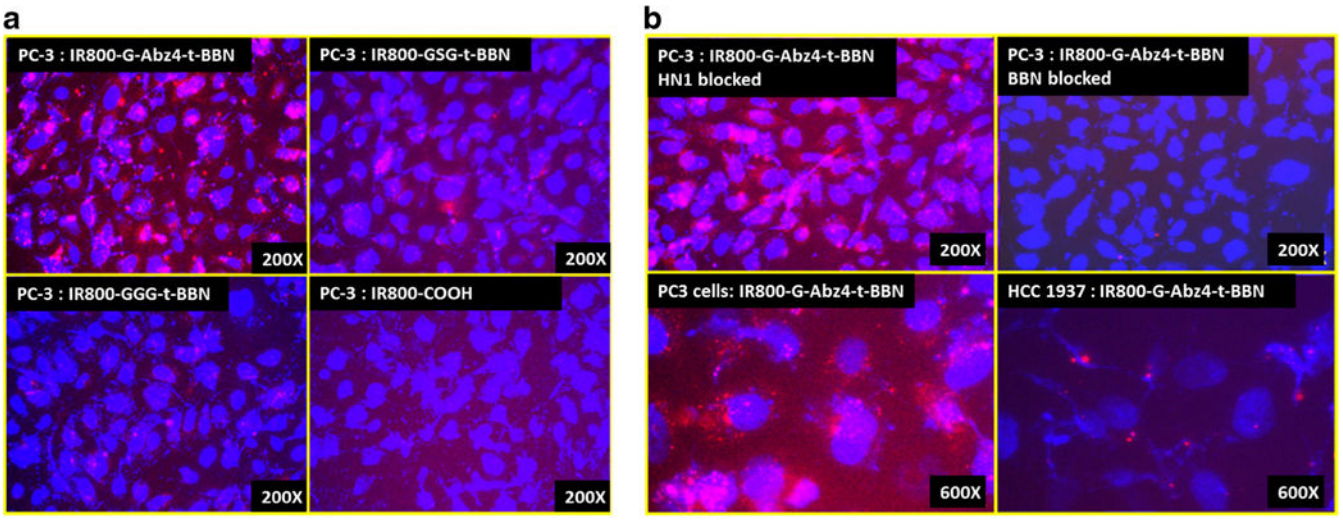

Fig. 3.

a Direct binding of IR800-G-Abz4-t-BBN, IR800-GSG-t-BBN, IR800-GGG-t-BBN, and IR800-carboxylate (dye control) to PC-3 cells detected by fluorescence microscopy. Nuclei are stained blue with DAPI; IR800 shows red. **b** IR800-G-Abz4-t-BBN binding to PC-3 cells blocked by BBN (*top right*) but not by HN1 (*top left*), a peptide that does not bind BBN-R. IR800-G-Abz4-t-BBN binds to PC-3 (*bottom left*) cells but not to BBN-R-negative HCC1937 cells (*bottom right*).

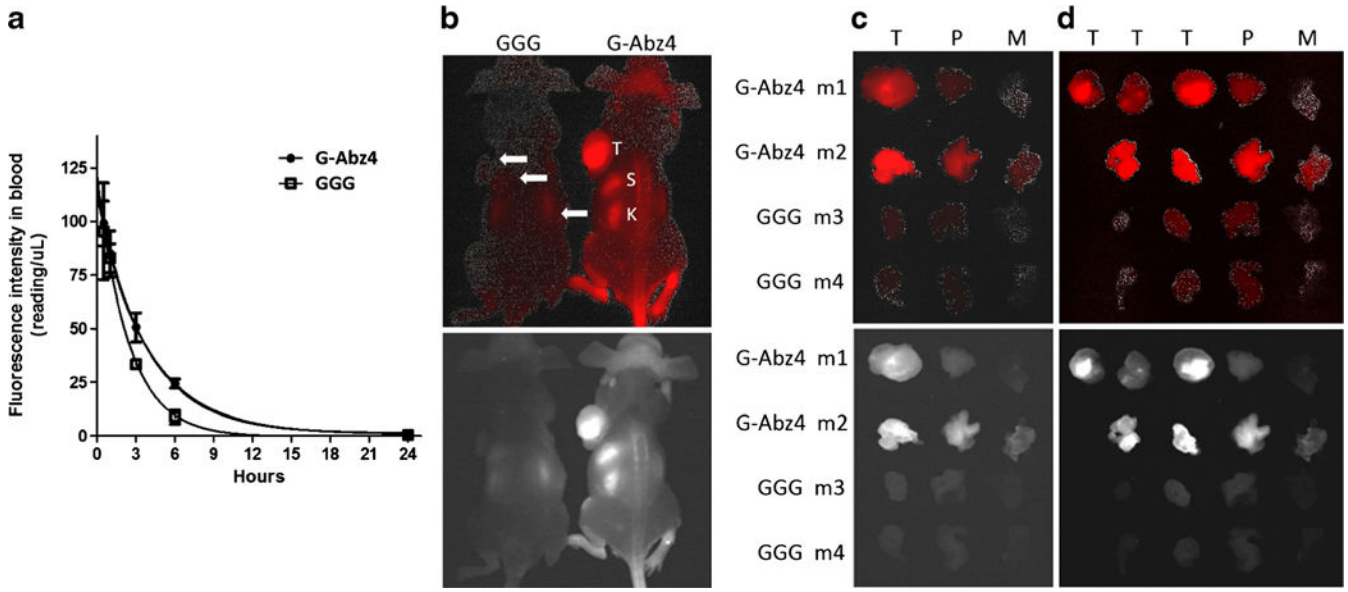

Fig. 4.

a Blood concentration vs time curves for IR800-GGG-t-BBN and IR800-G-Abz4-t-BBN in balb/c mice. **b**, **c**, **d** CRi images (*top*, *red*) and Fluobeam images (*bottom*, *white*) of nude mice-bearing PC-3 xenograft tumors, 24-h post-intravenous dose of 10 nmol. **b** Whole body images of mice 1 and 3, showing tumor (*T*), spleen (*S*), and kidneys (*K*). **c** Excised whole tumor (*T*), pancreas (*P*), and muscle (*M*). **d** The same tumors from **b**. Sliced into equal thicknesses (2 mm). Images for mice 5 and 6 are in Supplemental Information, Figs. 6.

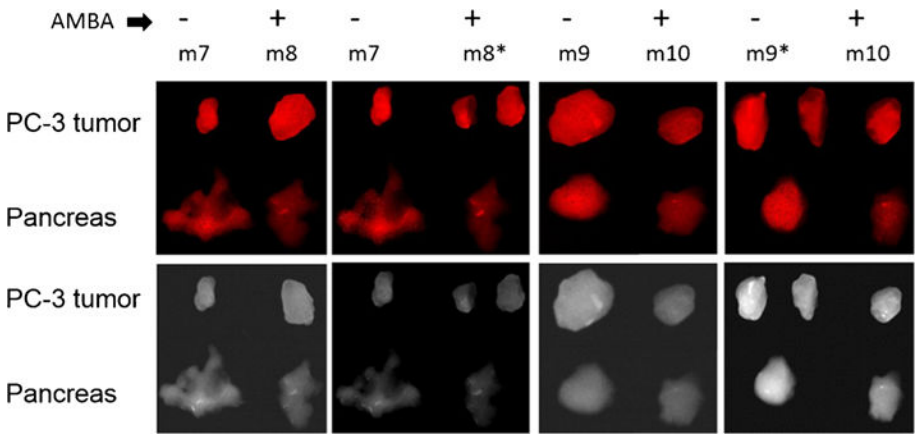

Fig. 5.

Nude mice (m7-12)-bearing PC-3 xenografts, intravenously dosed at 10 nmol IR800-Abz4-t-BBN alone (mice marked *minus sign*) or coinjected with 100 nmol AMBA (mice marked *plus sign*). Tumor and pancreas were excised at 3-h post-dose and imaged by CRi (*top*, *red*) and Fluobeam (*bottom*, *white*). AMBA visibly diminished binding to pancreas but not tumor. *Asterisks* larger tumors in m8 and m9 were cut into sizes similar to m7 and m10. In m7 and m8 the pancreas are spread out; in m9 and m10, the pancreas are piled up. M11 and m12 not shown.

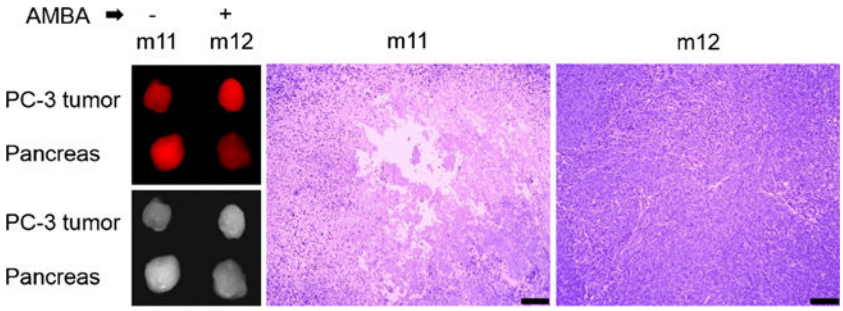

Fig. 6.

The unblocked tumor in mouse 11 (m11) from the blocking experiment in Fig. 5 appeared low in signal relative to its high signal pancreas in CRi (*top panel*) and Fluobeam (*bottom panel*). Histology of a central cut through the tumors of m11 and m12 demonstrated necrotic areas only in the tumor of m11 (*bar* is 200 microns).

Table 1

IC_{50} data (nM) against $^{125}Ityr_4$-BBN in live cultured cells

Fluor	Linker	PC-3	T47D	AR42-J	Ref.
Carbocyanine	GSG	–	–	1.8±0.2	[36]
AF680	GGG	8.2±1.2	7.7±1.4		[37, 45]
IR800	G-Abz4	2.6±0.2	3.1±1.1		This work
IR800	GSG	56±5	57.4±1.2		This work
IR800	GGG	187±31	383±1.0		This work
BBN	None	0.8±1.4	1.7±1.1		This work

AR42-J are rat pancreatic acinar cells known to possess BBN-R